



저작자표시-비영리-동일조건변경허락 2.0 대한민국

이용자는 아래의 조건을 따르는 경우에 한하여 자유롭게

- 이 저작물을 복제, 배포, 전송, 전시, 공연 및 방송할 수 있습니다.
- 이차적 저작물을 작성할 수 있습니다.

다음과 같은 조건을 따라야 합니다:



저작자표시. 귀하는 원저작자를 표시하여야 합니다.



비영리. 귀하는 이 저작물을 영리 목적으로 이용할 수 없습니다.



동일조건변경허락. 귀하가 이 저작물을 개작, 변형 또는 가공했을 경우에는, 이 저작물과 동일한 이용허락조건하에서만 배포할 수 있습니다.

- 귀하는, 이 저작물의 재이용이나 배포의 경우, 이 저작물에 적용된 이용허락조건을 명확하게 나타내어야 합니다.
- 저작권자로부터 별도의 허가를 받으면 이러한 조건들은 적용되지 않습니다.

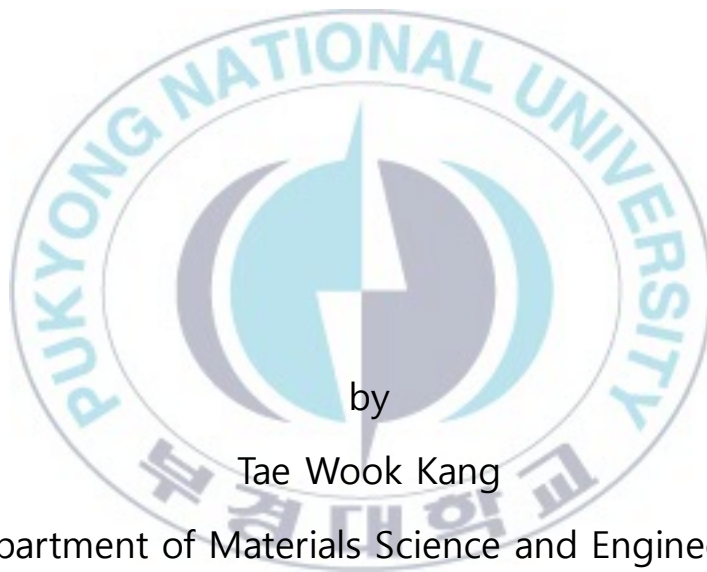
저작권법에 따른 이용자의 권리는 위의 내용에 의하여 영향을 받지 않습니다.

이것은 [이용허락규약\(Legal Code\)](#)을 이해하기 쉽게 요약한 것입니다.

[Disclaimer](#)

Thesis for the Degree of Master of Engineering

# Yellow YAG:Ce Single Crystal Phosphor for High-power LD/LED



by

Tae Wook Kang

Department of Materials Science and Engineering

The Graduate School

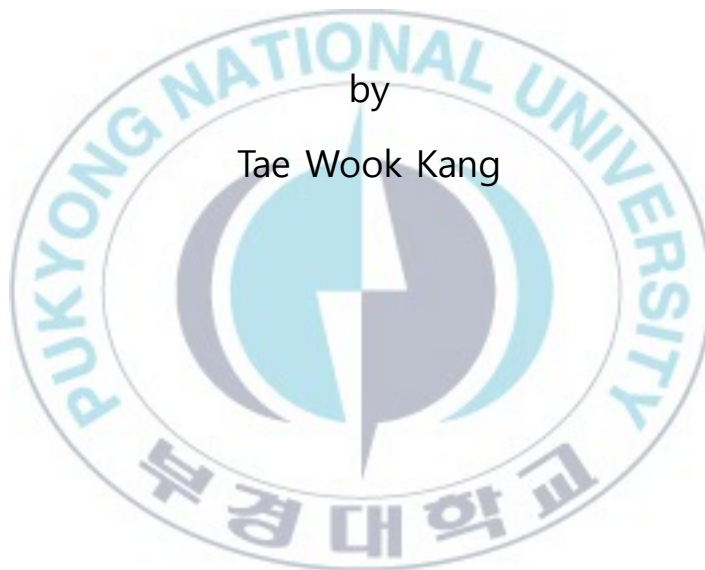
Pukyong National University

February 2015

# Yellow YAG:Ce Single Crystal Phosphor for High-power LD/LED

(고출력 LD/LED 용 황색 YAG:Ce 단결정 형광체)

Advisor : Prof. Hee Lack Choi



A thesis submitted in partial fulfillment of the requirements  
for the degree of  
Master of Engineering  
in Department of Materials Science and Engineering, The Graduate School,  
Pukyong National University

February 2015

# Yellow YAG:Ce Single Crystal Phosphor for High-power LD/LED

A dissertation

by

Tae Wook Kang

Approved by:

---

(Chairman) Chan Park

---

(Member) Jong Su Kim

(Member) Hee Lack Choi

February 27, 2015

# Contents

<b>Abstract</b> .....	
<b>1. Introduction</b> .....	1
<b>2. Background</b> .....	3
2.1. Phosphor for White light generations.....	3
2.2. $\text{Y}_3\text{Al}_5\text{O}_{12}:\text{Ce}^{3+}$ (YAG:Ce).....	5
2.2.1. Garnet structure.....	5
2.2.2. Luminescent properties of $\text{Ce}^{3+}$ .....	6
2.3. Floating Zone Technique.....	8
2.3.1. Image Furnace.....	8
2.3.2. Basic principle.....	9
<b>3. Experimental</b> .....	12
3.1. Making feed rod.....	12
3.2. Crystal Growth.....	13
3.3. Measurements of properties.....	13
<b>4. Results and Discussions</b> .....	14
4.1. Growth crystal .....	14
4.2. Luminescence properties of YAG:Ce single crystal .....	16
4.3. Temperature dependence.....	19

5. Conclusion .....	32
References.....	33
국문 요약.....	35



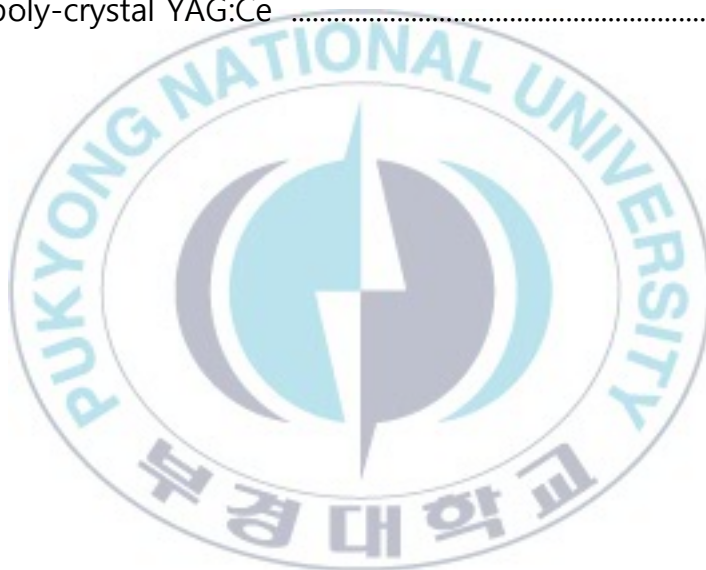
## List of Figures

Fig. 1. Three types of White LEDs; (a) RGB individual LEDs, (b) blue LED and YAG:Ce yellow phosphor, (c) UV LED and RGB phosphor.....	4
Fig. 2. Crystal structure of yttrium-aluminum garnet structure .....	5
Fig. 3. The position of $Y^{3+}$ , $Al^{3+}$ , $O^{2-}$ ions in garnet structure .....	6
Fig. 4. The effect of the crystal field interaction on the free $Ce^{3+}$ energy states .....	7
Fig. 5. Schematic diagram of floating zone system .....	9
Fig. 6. Crystal growth process steps in floating zone method .....	10
Fig. 7. The sequence of fabrication of feed rod .....	12
Fig. 8. The photograph of sliced YAG:Ce single crystal .....	14
Fig. 9. XRD patterns of (a) the sliced YAG:Ce sample (the {110} orientation group) and (b) the samples of YAG:Ce powder .....	15
Fig. 10. YAG:Ce single crystal and commercial powder (a) PL spectra, (b) PLE spectra .....	17
Fig. 11. PL spectra (a) with varying $Ce^{3+}$ concentration, (b) with substituting Lu ions in Y sites .....	18
Fig. 12. Temperature dependent PL spectra of (a) single-crystal, (b) poly-crystal, and (c) temperature dependence of the relative PL intensity .....	19-20
Fig. 13. Comparison with Raman spectra of single-crystal and poly-crystal YAG:Ce phosphors at (a) total, (b) 1 phonon, (c) 2 phonon, and (d) 3 phonon range .....	22-23

Fig. 14. Temperature-dependent Raman spectra of single-crystal YAG:Ce at (a) total, (b) 1 phonon, (c) 2 phonon, and (d) 3 phonon range..... 26-27

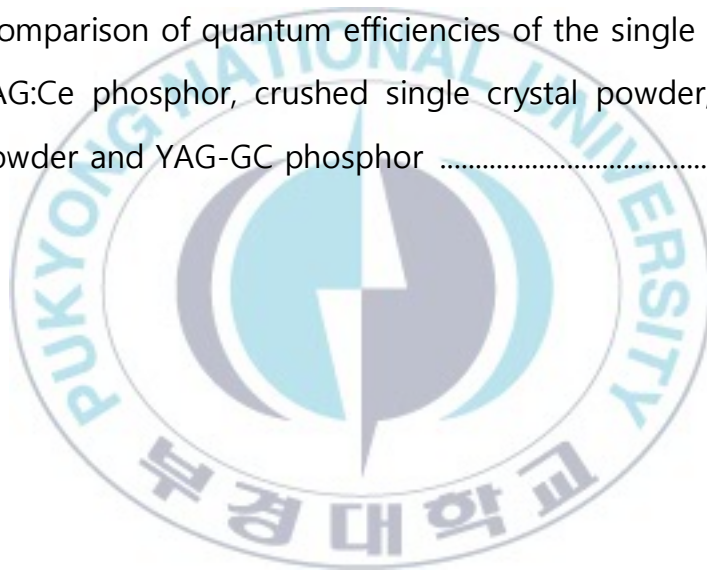
Fig. 15. Temperature-dependent Raman spectra of commercial powder at (a) total, (b) 1 phonon, (c) 2 phonon, and (d) 3 phonon range ..... 28-29

Fig. 16. Thermographic images of (a) single-crystal and (b) poly-crystal YAG:Ce ..... 31



## List of Tables

Table. 1. Effect of parameters during FZ growth.....	11
Table. 2. Growth conditions and Specimens.....	13
Table. 3. Comparison between experimental and calculated Raman- active shifts in 1 phonon range .....	24
Table. 4. The calculated thermal conductivity ratio .....	30
Table. 5. Comparison of quantum efficiencies of the single crystal YAG:Ce phosphor, crushed single crystal powder, commercial powder and YAG-GC phosphor .....	31



# Yellow YAG:Ce Single Crystal Phosphor for High-power LD/LED

Tae Wook Kang

Department of Materials Science and Engineering  
The Graduate School  
Pukyong National University

## Abstract

Yellow-emission  $Y_3Al_5O_{12}:Ce$  (YAG:Ce) single crystal phosphors was grown through a floating zone method. They had the {110} crystal orientations in the cubic structure. It showed a yellow photoluminescence spectrum with 540 nm peak and 75 nm half width, and a blue photoluminescence excitation spectrum with 450 nm peak due to f-d transition of  $Ce^{3+}$  ion. The Lu substitutions for Y were tried for emission color tuning: the color shifted to the green as an increase of Lu compositions. Its optical and thermal properties are compared with the commercial YAG:Ce powder. The Raman intensity are significantly increased for a single crystal YAG phosphor. Thus, Raman spectroscopic studies on the YAG can be helpful to estimate the thermal conductivity. It gave an excellent thermal stability in photoluminescence under high-power laser diode due to its high thermal conductivity, especially at the high temperature.

---

**Keyword :**  $Y_3Al_5O_{12}:Ce$  phosphor, single crystal, floating zone method, thermal quenching, laser dio

## 1. Introduction

Conventional lamps rely on either incandescence or discharge in gases. These are associated with large energy losses that are essentially inherent because the high temperatures and large Stokes shifts involved. The development of visible and light emitting diodes (LEDs) that exhibit efficiencies comparable or higher than those of conventional lamps gave birth to new lighting technology [1].

White LEDs as a next generation light source have significant interest in the global market due to their outstanding characteristics such as nonpollution, low power consumption, long life time and high brightness, reliability compared to conventional light source. Moreover, white LEDs have been the interesting subject due to their potential applications in indicators, automobile headlights, and general illumination [2].

The strategies involved in developing white LED are (i) the combination of a blue LED with a yellow phosphor and red, green phosphors; (ii) the combination of UV-LED with blue, green, and red phosphors; (iii) the combination of blue, green, and red LEDs. Up to now, the conventional method for making white light is to combine a blue LED with a yellow phosphor because of the lowest manufacturing costs at present and capability to promote high light yield. This type composed of a blue InGaN-based LED and a yellow-emitting  $\text{Y}_3\text{Al}_5\text{O}_{12}:\text{Ce}^{3+}$  (YAG:Ce). The most famous yellow-emission YAG:Ce phosphors were reported in 1967 with their primary use in cathode-ray tubes. They were used as a color conversion phosphor in white-light-emitting diodes by NICHIA Company in 1996 [3].

YAG:Ce phosphor efficiently converts InGaN-based blue LED radiation into a very broad intense yellow emission band due to the 4f-5d transition of the  $\text{Ce}^{3+}$  ion and shows a maximum absorbance in the blue region. White light is then a result of the combination of the yellow emission with the non-absorbed blue emission from the

blue LED.

Recently, for high-power LEDs or laser diodes (LD) (>1 Watt per single package), the conventional structure with yellow phosphor powders dispersed in the organic epoxy resin exhibit a significant drop in efficiency at high blue irradiations and high temperatures (100 °C ~ 150 °C). It is due to burning of organic epoxy resin as well as blackening of phosphor surface [4]. The YAG:Ce has the excellent thermal conductivity (~ 13 W/mK) compared with other silicate phosphors (~ 1.5 W/mK). The high thermal conductivity prevents local heating from a concentrated high-power blue irradiation and provide a good lumen maintenance at a high temperature (~ 90 % at 150 °C), and thus a long lifetime is expected. In order to solve this problem, new type phosphor conversion materials, which do not require the presence of epoxy resin, were suggested: (i) polycrystalline YAG:Ce transparent ceramics [5]; (ii) low temperature glass mixture with YAG:Ce phosphor plates [6]; (iii) Ce,Gd:YAG single crystal phosphor plates (SCPPs) [7]. This means that development of LEDs requires research on phosphors used for white LEDs.

The thermal conductivity in crystalline dielectric solids is mainly by way of lattice vibrations (phonons). Raman scattering is a direct method for evaluating the phonon modes and its accuracy is a function of the Raman intensity. The Raman intensity are significantly increased for a single crystal YAG phosphor. Thus, Raman spectroscopic studies on the YAG can be helpful to estimate the thermal conductivity. Its Raman spectrum has contain 25 modes ( $3A_{1g}+8E_g+14T_{2g}$ ), and its infrared spectrum contains 17  $T_{1u}$  modes.

Therefore, in this work, yellow YAG:Ce single crystal phosphor was grown through a floating zone method. The yellow YAG:Ce single crystal phosphor was pumped by a high-power blue LED and laser diode (LD) for a white light source. Its optical and thermal properties are compared with the commercial YAG:Ce powder.

## 2. Background

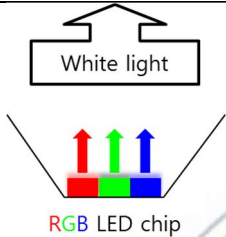
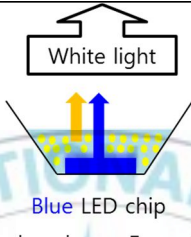
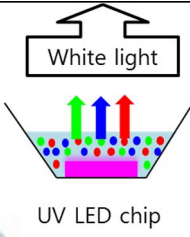
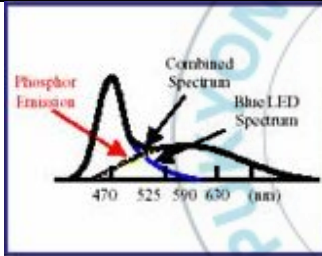
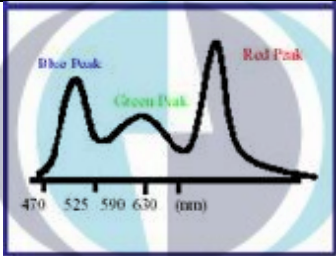
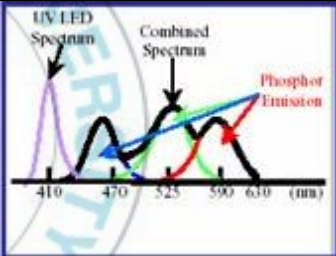
### 2.1. Phosphor for White light generations

Traditional incandescent and fluorescent lamp for general illumination can be replaced by the solid-state lighting. Therefore, white LEDs with properties superior to those of traditional light sources, such as high luminous efficiency, tunable color temperatures, high color rendering properties, and long lifetime, are continuously pursued. Although the first red LED was developed in 1968, the first white LED was made with invention of efficient blue LED in the 1990s [8].

Presently three types of white LEDs have been proposed and manufactured. The device structures of three types white LEDs are shown in Figure 1. First type was composed of a blue LED chip and a yellow-emitting phosphor. In 1991, Nichia Corporation invented the development of blue LEDs based on InGaN. White LED composed of a blue LED and a yellow emitting  $Y_3Al_5O_{12}:Ce^{3+}$ (YAG:Ce) was first commercialized in 1996 [9]. It was the most common and simple technology. This type has captured a substantial market because of their attractive properties such as reduce power consumption, compactness, efficient light output, reliability, and longer lifetime.

Second, a combination of two or more phosphors, spanning the blue to red spectrum, is applied to a UV or violet LED. In the past few years, high-power UV LEDs have been developed by a number of companies and institutions. Since then the research and development of phosphors, which can be excited by UV LEDs, emitting the three primary colors, blue, green, and red, has stimulated.

The last type was that three LEDs of the primary colors are combined with each other. It requires at least three LEDs, and each device must be adjusted by individual supply circuits to balance the emission intensity of each color for proper white light generation because of varying brightness of the different wavelength emitting LEDs.

All semiconductor-based illumination device	Semiconductor/phosphor devices	
(a) RGB LED Chip	(b) Blue LED Chip + Yellow phosphor	(c) UV LED Chip + RGB phosphor
 <p>White light</p> <p>RGB LED chip</p>	 <p>White light</p> <p>Blue LED chip Yellow phosphor + Epoxy/Silicon</p>	 <p>White light</p> <p>UV LED chip RGB phosphor + Epoxy/Silicon</p>
		
<ul style="list-style-type: none"> <li>➤ Potentially highest efficiency</li> <li>➤ Very large color gamut</li> <li>➤ Tunable white point</li> </ul>	<ul style="list-style-type: none"> <li>➤ The most simple technology</li> <li>➤ Decent color rendering (Ra~80)</li> </ul>	<ul style="list-style-type: none"> <li>➤ White point determined by phosphors only</li> <li>➤ Excellent color rendering</li> </ul>
<ul style="list-style-type: none"> <li>➤ Green LED efficiency is low</li> <li>➤ Temperature stability of LEDs depends on color</li> <li>➤ Individual supply circuits</li> </ul>	<ul style="list-style-type: none"> <li>➤ Reduced extraction efficiency</li> <li>➤ "Quantum deficit" is fundamental</li> <li>➤ Blue LED + YAG phosphor : High CCT and limited color rendering</li> <li>➤ UV LED + RGB phosphor : Degradation of organic encapsulants</li> </ul>	

**Fig. 1.** Three types of White LEDs; (a) RGB individual LEDs, (b) blue LED and YAG:Ce yellow phosphor, (c) UV LED and RGB phosphor

## 2.2. $\text{Y}_3\text{Al}_5\text{O}_{12}:\text{Ce}^{3+}$ (YAG:Ce)

### 2.2.1. Garnet structure

$\text{Y}_3\text{Al}_5\text{O}_{12}:\text{Ce}^{3+}$  phosphor belongs to the garnet structure and has been called yttrium-aluminum garnet (YAG). It is a species of cubic structures, general formula is marked as  $\text{Y}_3\text{Al}_2\text{Al}_3\text{O}_{12}$ . The unit cell is formed by eight formula units. There are 160 atoms in the unit cell. The O polyhedra define three kind of cation site; dodecahedral (eight-fold), octahedral (six-fold) and tetrahedral (four-fold). The Y ions occupy the 24 sites. Each Y ion is dodecahedral coordinated to eight O atoms situated at the corners of a distorted cube. There are two different sites for Al ion. The Al ions occupy the 16 sites with octahedral point symmetry, and the 24 sites with tetrahedral point symmetry. The Ce ion is incorporated into the YAG host material by replacing the Y ion [10]. Garnet structure and positions of  $\text{Y}^{3+}$ ,  $\text{Al}^{3+}$ ,  $\text{O}^{2-}$  ions are shown in Figure 2 and 3.

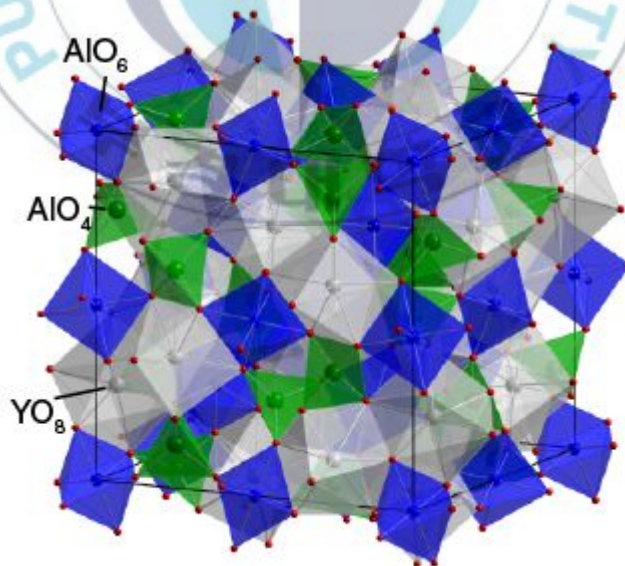


**Fig. 2.** Crystal structure of yttrium-aluminum garnet structure

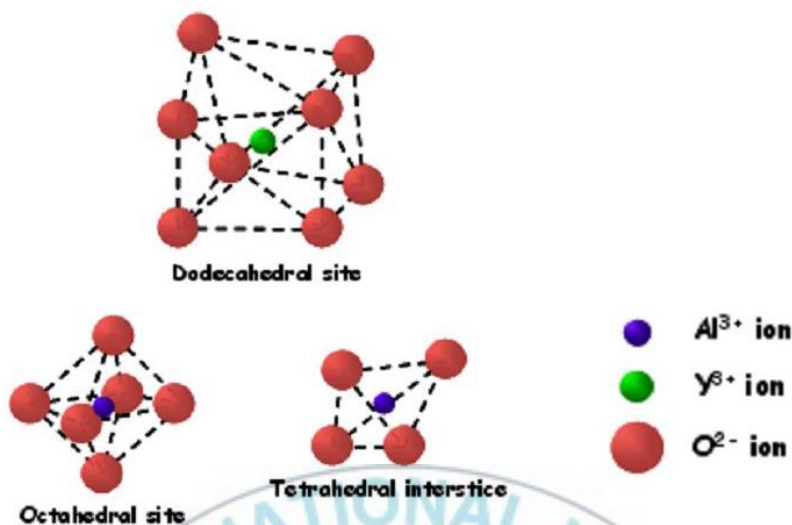


Fig. 3. The position of  $Y^{3+}$ ,  $Al^{3+}$ ,  $O^{2-}$  ions in garnet structure

### 2.2.2. Luminescent properties of $Ce^{3+}$

$Ce^{3+}$  ion ( $4f^1$ ) is the most simple example, since it is a one-electron case. The excited configuration is  $5d^1$ . The  $4f^1$  ground state configuration yields two levels, i.e.  $^2F_{5/2}$  and  $^2F_{7/2}$  separated by some  $20000\text{cm}^{-1}$  due to spin-orbital coupling. The  $5d^1$  configuration is split by the crystal field in 2 to 5 components. The total splitting amounts to some  $15000\text{cm}^{-1}$ . The luminescence photon energy depends strongly on the structure of the host crystal through the crystal field splitting of the  $5d$  state, as shown in Figure 4 and varies from near-ultraviolet to the greenish yellow region. The emission occurs from the lowest crystal field component of the  $5d^1$  configuration to the two levels,  $^2F_{5/2}$  and  $^2F_{7/2}$ , of the ground state. This gives the  $Ce^{3+}$  emission its typical double-band shape. Figure 4 shows a schematic diagram of the effect of the crystal field interaction on the  $Ce^{3+}$  ion and the Stokes shift of the  $Ce^{3+}$  emission transitions.

The Stokes shift of the  $Ce^{3+}$  emission is never very large and varies from a thousand to a few thousand wave numbers. The spectral position of the emission band depends on three factors; (i) covalency which will reduce the energy difference

between the  $4f^1$  and  $5d^1$  configurations, (ii) crystal field splitting of the  $5d^1$  configuration: a large low-symmetry crystal field will lower the lowest crystal field component from which the emission originates, and (iii) the Stokes shift. Usually, the  $Ce^{3+}$  emission is in the ultraviolet or blue spectral region, but in YAG it is in the green and red due to crystal field effect.

The decay time of the  $Ce^{3+}$  emission is  $10^{-7}$  to  $10^{-8}$  s, the shortest in observed lanthanide ions. This is due to two reasons: the  $d \rightarrow f$  transition is both parity-allowed and spin allowed since  $4f^1$  and  $5d^1$  states are spin doublets, i.e. the emission transition is a fully allowed one [11].

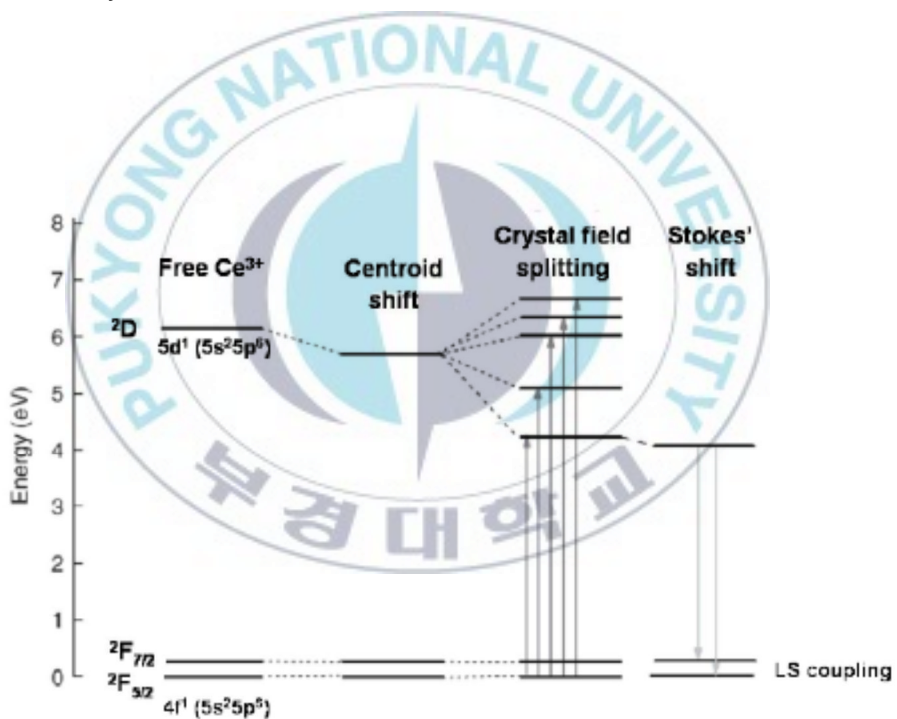


**Fig. 4.** The effect of the crystal field interaction on the free  $Ce^{3+}$  energy states

## 2.3. Floating Zone Technique

### 2.3.1. Image Furnace

Following extensive development, in particular at NEC in Japan and the University of Freiburg in Germany, image furnaces became commercially available in the 1980s [12, 13].

The image furnace used in the experiment is NEC SC-35HD. Figure 5 shows the most important part of the furnace and demonstrates how high temperature is obtained. The furnace has two ellipsoidal or parabolic reflectors, it is used to focus the light from halogen or xenon lamps onto a vertically held rod shaped sample to produce a melting zone, i.e. the light from the lamps is reflected by the inner surface and then focused at the common focal point. A seed and a feed material rod are placed in a quartz tube. The gap between the two rods is placed at the common focal point where the temperature can be as high as 2200 °C, depending on factors such as the sample color, lamp power, and the voltage level applied on the two lamps. When growing, the two rods rotate in opposite directions and move simultaneously downwards. The feed rod melts at the focal point; the melt crystallizes after moving out of the melting zone. The whole processes are protected by a quartz tube; thus proper atmosphere and pressure can be easily controlled. The crystal growth status can be monitored on a small screen through an optical lens [14, 15].

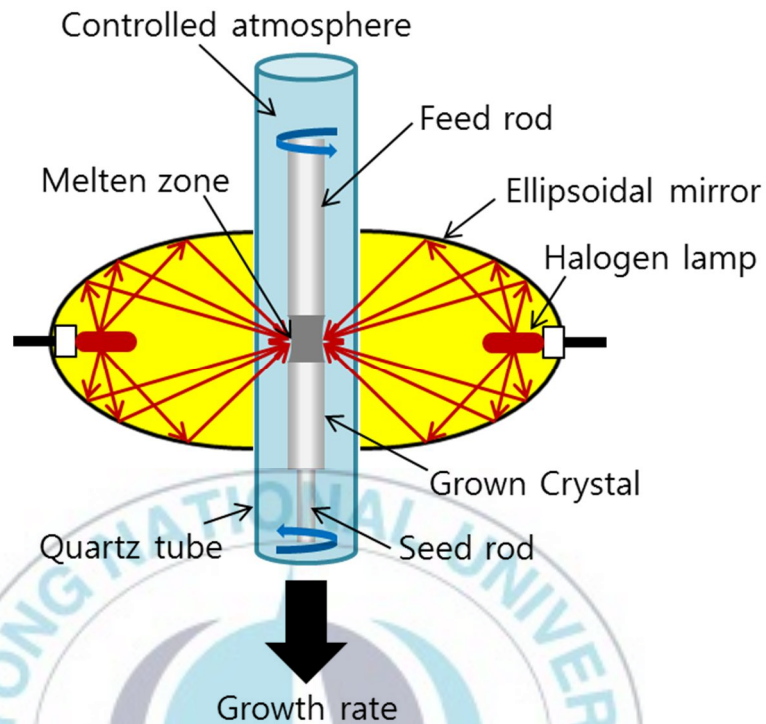


**Fig. 5.** Schematic diagram of floating zone system

### 2.3.2. Basic principle

The basic idea of float zone (FZ) technique is to move the melting zone over the seed rod. This method was first used to purify the sample, taking advantage of the small segregation coefficients of many impurities. The impurities contained in the feed material would then prefer to remain in the melting zone, not in the crystallized parts. After moving the seed rod with the melting zone, the crystallized parts will be purified. If the condition is correct, the crystallized parts will form a single crystalline phase.

The important point to successfully grow a single crystal with FZ is to maintain the melting zone. If the growth condition is not correct, the melting zone will not be maintained. For example, if the temperature is too high and low, the melting zone between the seed and feed will be disconnected [16]. Table 1 is shown effects of

parameters during FZ growth [15]. In addition, crystal growth process steps are described by Figure 6.

Compared with other methods, the FZ method has the following advantages:

- (i) no crucible necessary, no contamination from the crucible;
- (ii) can control the gas atmosphere and pressure easily;
- (iii) large temperature gradient on the crystallization process;
- (iv) steady-state process of the crystal growth

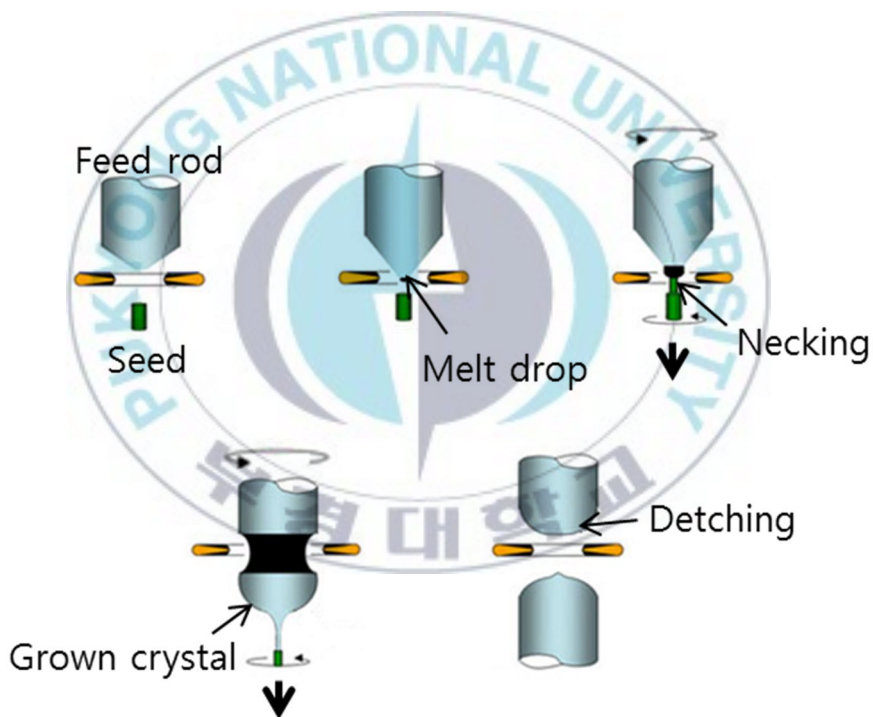


**Fig. 6.** Crystal growth process steps in floating zone method

**Table. 1.** Effect of parameters during FZ growth

<b>Parameter</b>	<b>Effect</b>
Feed rod	<ul style="list-style-type: none"><li>➤ A poorly compacted feed rod can lead to bubble formation in the growing crystal.</li></ul>
Crystallization rate	<ul style="list-style-type: none"><li>➤ Crystal growth at lower growth rates generally yields larger crystals.</li><li>➤ Crack formation is reduced when lower growth rates are used</li><li>➤ With many materials, growth rates are slowed.</li></ul>
Growth atmosphere and gas pressure	<ul style="list-style-type: none"><li>➤ Increasing the gas pressure is reported to increase the lamp power needed to melt the sample and reduce the melting zone stability.</li><li>➤ Depending on the material, different growth atmospheres and gas pressures are required.</li></ul>
Temperature gradient and melting zone temperature	<ul style="list-style-type: none"><li>➤ Larger temperature gradients along the growth direction are more likely to cause cracking in the growing crystal due to thermal stresses.</li><li>➤ A lower melting zone temperature can help to prevent evaporation of components during growth and give a more homogeneous crystal.</li></ul>
Rotation rate	<ul style="list-style-type: none"><li>➤ Rotation is usually used to ensure efficient mixing in the melting zone.</li><li>➤ Higher rotation rate can be a way of lowering the convexity of the interface, so giving a more stable melting zone.</li></ul>

### 3. Experimental

#### 3.1. Making feed rod

For a successful crystal growth, the feed rod should be dense, uniform, and have the right composition. A uniform rod has nearly constant diameter, density and homogeneous chemistry, which is critical to keep the melting zone stable.

Figure 7 shows the process of making feed rod.  $Y_2O_3$  (High Purity chemicals, 99.99 %),  $Al_2O_3$  (High Purity chemicals, 99.99 %) and  $CeO_2$  (High Purity chemicals, 99.9 %) were used as the starting materials.  $Y_2O_3$  and  $Al_2O_3$  powders were weighted and mixed at the stoichiometric ratio;  $CeO_2$  was added to be 0.1 at%, 0.5 at% and 1 at%, respectively. Then, mixed powder goes through forming process by using cold isostatic press (CIP) under  $2000\text{kg}/\text{cm}^2$ . These rods were then sintered at  $1500\text{ }^\circ\text{C}$  for 4h under reducing atmosphere.

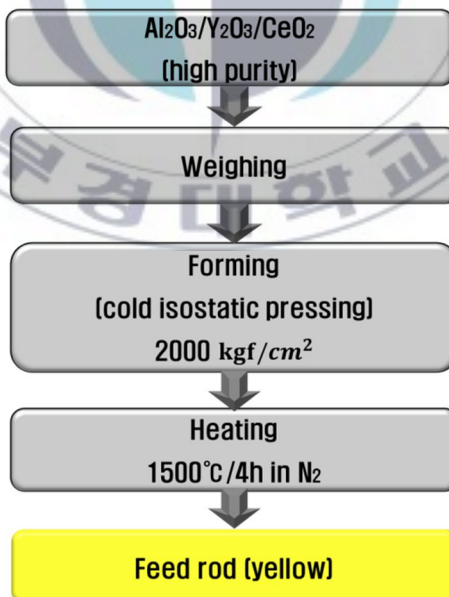


Fig. 7. The sequence of fabrication of feed rod

### 3.2. Crystal Growth

Seed rod and sintered feed rod install by using a thin wire (platinum wire of 0.3 mm diameter) in the image furnace. At this time, Rods of seed and feed are mounted in the furnace so as to be perfectly aligned. Two halogen lamps (3.5 kW) are used in a heat source. Rods are heated and melted, and then crystal is grown under the growth condition. Crystal growth conditions and samples are simply shown by Table 1.

**Table. 2.** Growth conditions and Specimens

Growth conditions	Specimens
➤ Growth rate : 1 mm/h	Commercial YAG:Ce powder
➤ Feed rotation : 15 RPM	Single crystal YAG:Ce 1 at%
➤ Seed rotation : 10 RPM	Single crystal YAG:Ce 0.5 at%
➤ Atmosphere : N <sub>2</sub> gas (1-3 L/min)	Single crystal YAG:Ce 0.1 at%
	Single crystal (Lu,Y)AG:Ce 1at%
	Single crystal LuAG:Ce 1at%

### 3.3. Measurements of properties

The obtained single crystal were identified through X-ray diffraction (XRD) technique (Cu K $\alpha$ , D/MAX 2500) with Ni-filtered Cu K $\alpha$  radiation, counting times of 30 minutes from 20° to 80° and 2 $\theta$  steps of 0.02°. The photoluminescence (PL) and photoluminescence excitation (PLE) spectra were obtained using Hitachi F-4500 fluorescence spectrometer. The Raman spectra were measured by ocean optics spectrometer (QE65000).

## 4. Results and Discussions

### 4.1. Growth crystal

Figure 8 shows the photograph of YAG:Ce single crystal sliced by thickness of 1 mm. The as-grown single crystal was approximately 5 mm in diameter and 30 mm in length. It was free of any inclusion and crack, and transparent with bright yellow coloration due to the strong blue-green absorption from the  $5d \rightarrow 4f$  transition of  $Ce^{3+}$  ions and the yellow luminescence from the  $4f \rightarrow 5d$  transition of  $Ce^{3+}$  ions.

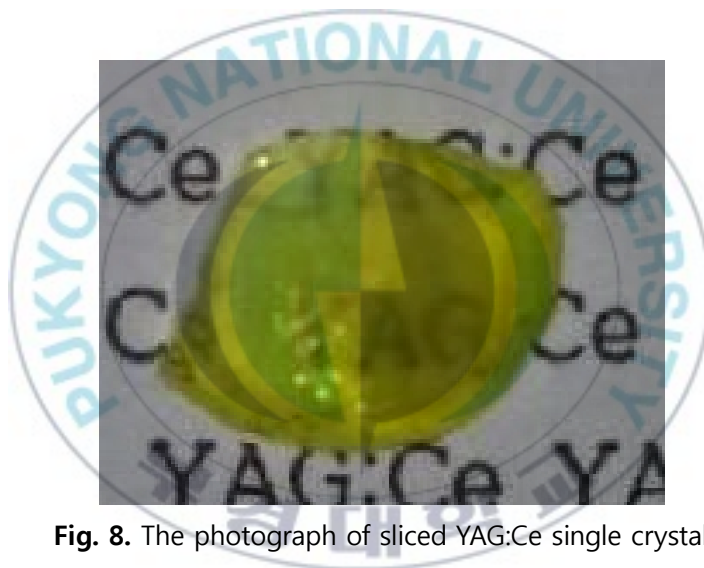


**Fig. 8.** The photograph of sliced YAG:Ce single crystal

Figure 9 shows XRD patterns of YAG:Ce phosphors sliced to the (110) orientation and crushed to the powder, synthesized powder by convention method, and the commercial powder sample. Figure 9 (b) XRD patterns are consistent with JCPDS Card (No. 73-1370). According to JCPDS Card No. 73-1370, the XRD patterns of the sample matched those of a cubic crystal structure with and  $Ia\bar{3}d$  (230) space group. The crushed YAG:Ce sample showed all crystal orientations like a conventional powder sample, while the sliced YAG:Ce sample showed only the {110} orientation group. The commercial powder sample showed the subequal XRD pattern of the single crystal

sample in terms of peak position. It is expected that the single crystal sample has the subequal chemical composition of the powder sample.

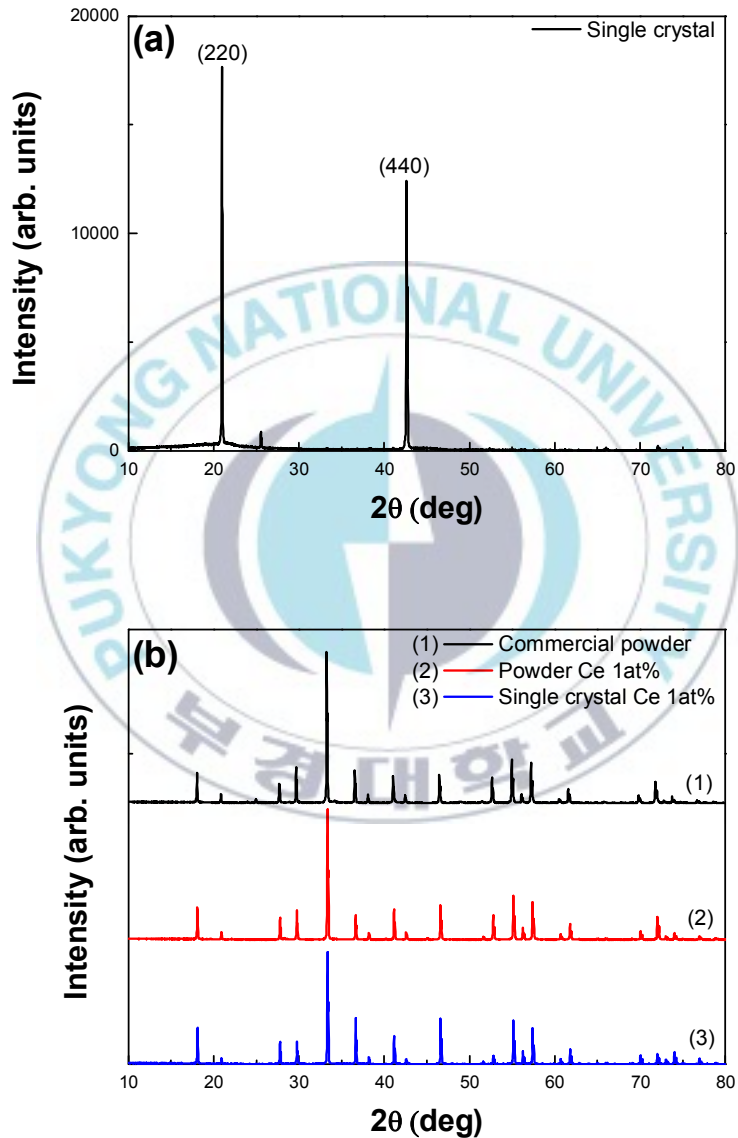


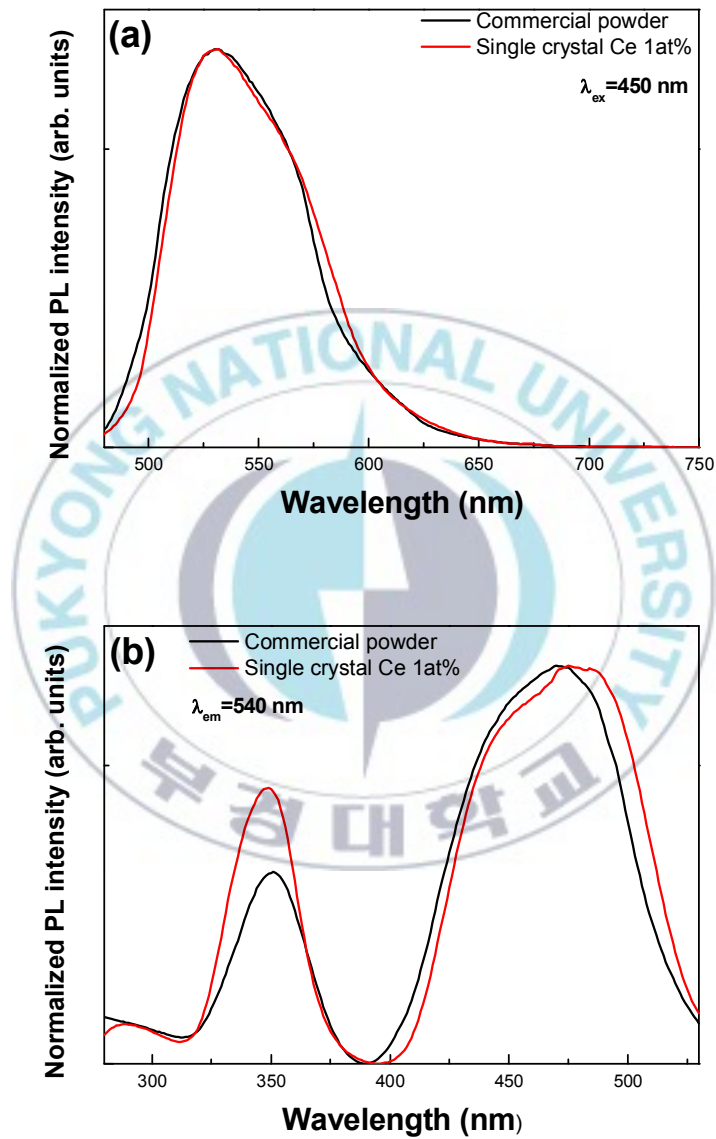
**Fig. 9.** XRD patterns of (a) the sliced YAG:Ce sample (the {110} orientation group) and (b) the samples of YAG:Ce powder

## 4.2. Luminescence properties of YAG:Ce single crystal

Figure 10 shows 540 nm-monitored PLE and 450 nm-excited PL spectra of YAG:Ce single crystal and the commercial powder. The both samples showed the almost same PL spectrum with peak position of 540 nm and half width of 75 nm. The same PL spectrum of both samples is attributed to their subequal chemical composition.

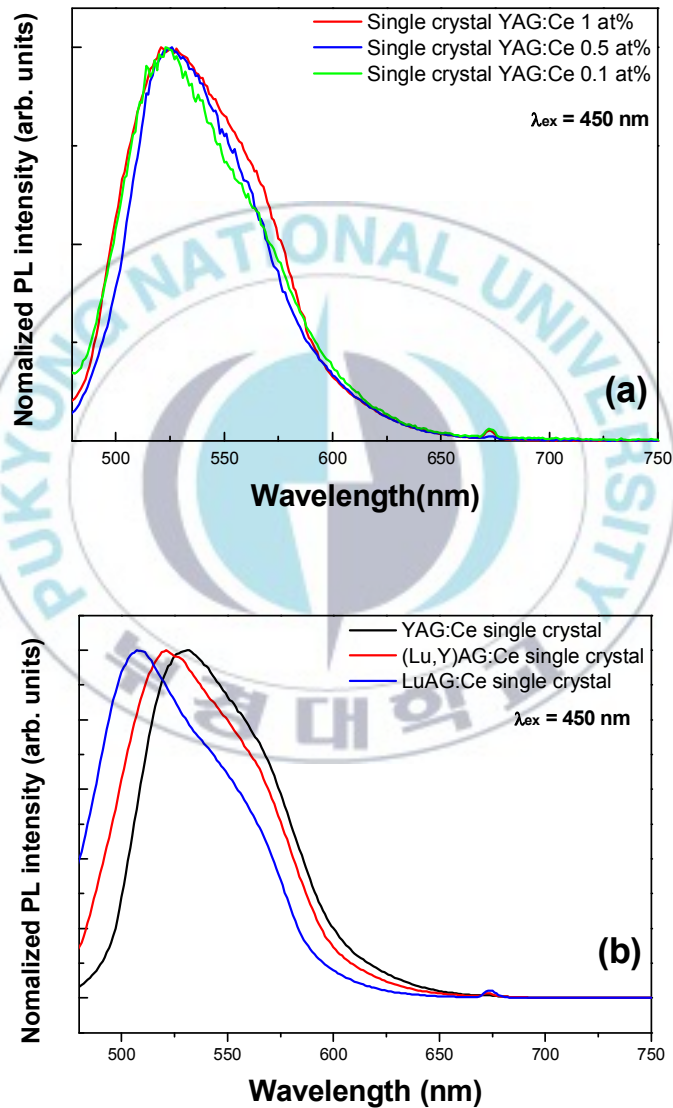
The Ce<sup>3+</sup> ions have the  $5s^25p^64f^15d^16s^2$  electron configuration. The  $4f^1$  ground state ( $^2F$ ) splits into two  $^2F_{5/2}$  and  $^2F_{7/2}$  levels due to the spin-orbit interaction. As a result, the PL spectral broadening is originated from overlapping of two emission peaks from the first lowest excited  $5d^1$  level to two spin-orbit split  $^2F_{5/2}$  and  $^2F_{7/2}$  levels of  $4f^1$  ground states.

The outer 5d electron extends spatially beyond the closed  $5s^25p^6$  shells, and the 5d levels are strongly affected by the crystal field from host lattice. The 5d orbital has a large crystal-field splitting together with decreasing the energy of the first lowest level: the first lowest (A) and the second lowest (B) levels. Thus, the 4f–5d transition energy shifts to the visible energy. For PLE spectra of both single crystal and the commercial powder as seen in Figure 10 (b), the one excitation band at 460 nm is attributed to the 4f–5d transition of Ce<sup>3+</sup> ions from the  $^2F_{5/2}$  level of 4f ground state to the first lowest 5d excited state (A). The other excitation band at 340 nm is due to the 4f–5d transition of Ce<sup>3+</sup> ions from the  $^2F_{5/2}$  level of 4f ground state to the second lowest 5d excited state (B).



**Fig. 10.** YAG:Ce single crystal and commercial powder (a) PL spectra, (b) PLE spectra

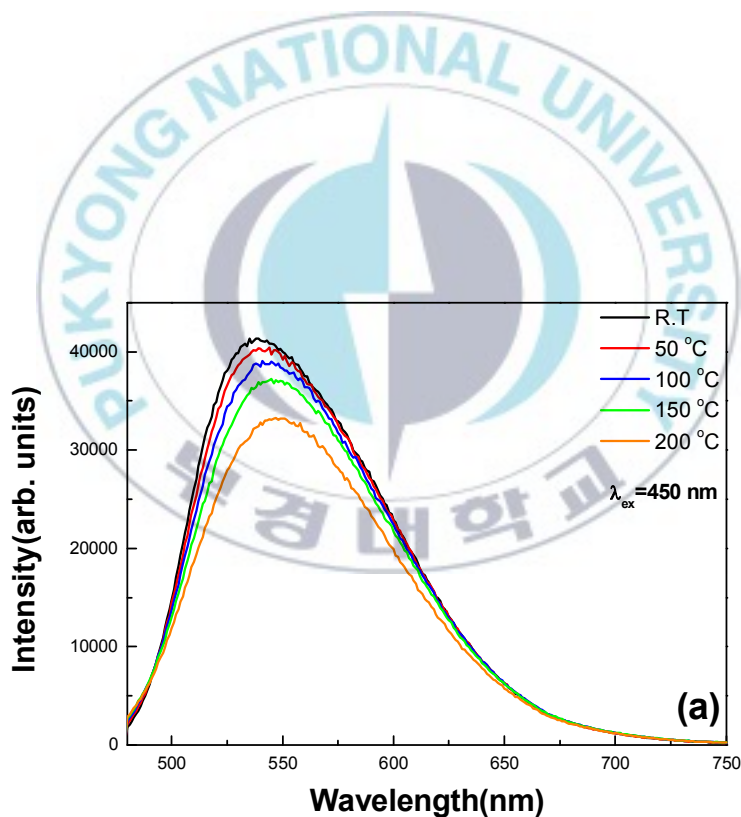
The PL spectra with varying  $\text{Ce}^{3+}$  concentration and substituting Lu ions in Y sites are shown in Figure 11. As  $\text{Ce}^{3+}$  concentration increased, so PL spectra are observed red-shift. In addition, the color shifted to the green by substitution of Lu ions in Y sites.

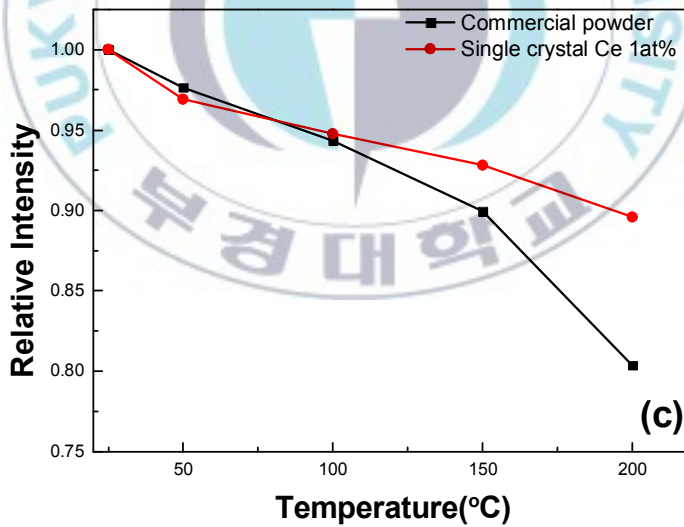
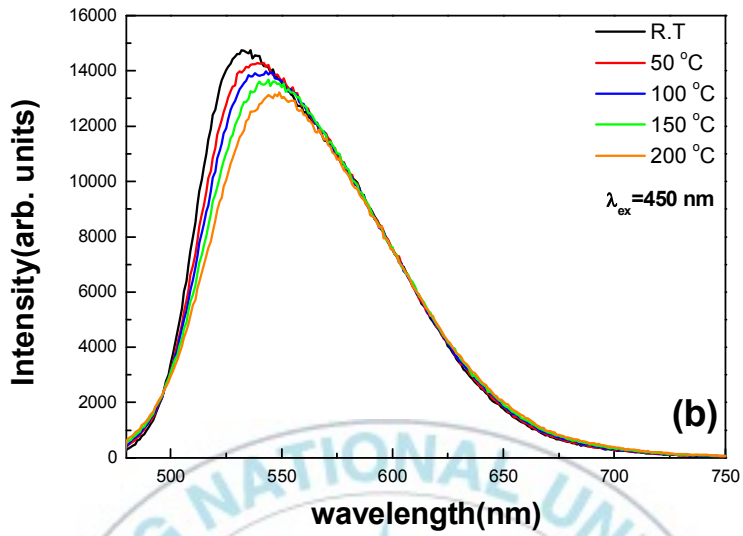


**Fig. 11.** PL spectra (a) with varying  $\text{Ce}^{3+}$  concentration, (b) with substituting Lu ions in Y sites

### 4.3. Temperature dependence

Figure 12 shows temperature-dependent PL spectra single-crystal and poly-crystal YAG:Ce phosphors, temperature dependence of the relative PL intensity. At the ambient temperature of 100 °C, both samples showed the slight thermal quenching behavior by 5 % of intensity drop. Above 100 °C, the quenching gap of both samples is significantly increased. At 200 °C, the decrease in PL intensity of the single crystal is 10 %. On the other hand, the decrease in PL intensity of the powder sample is 20 %.

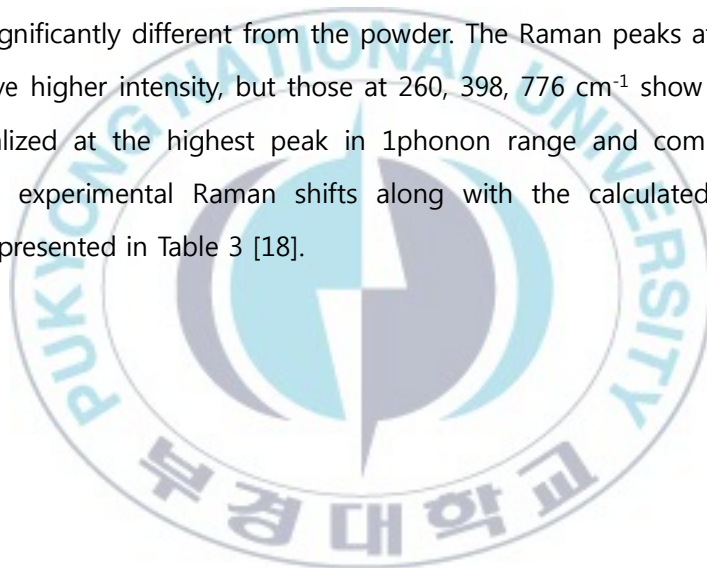


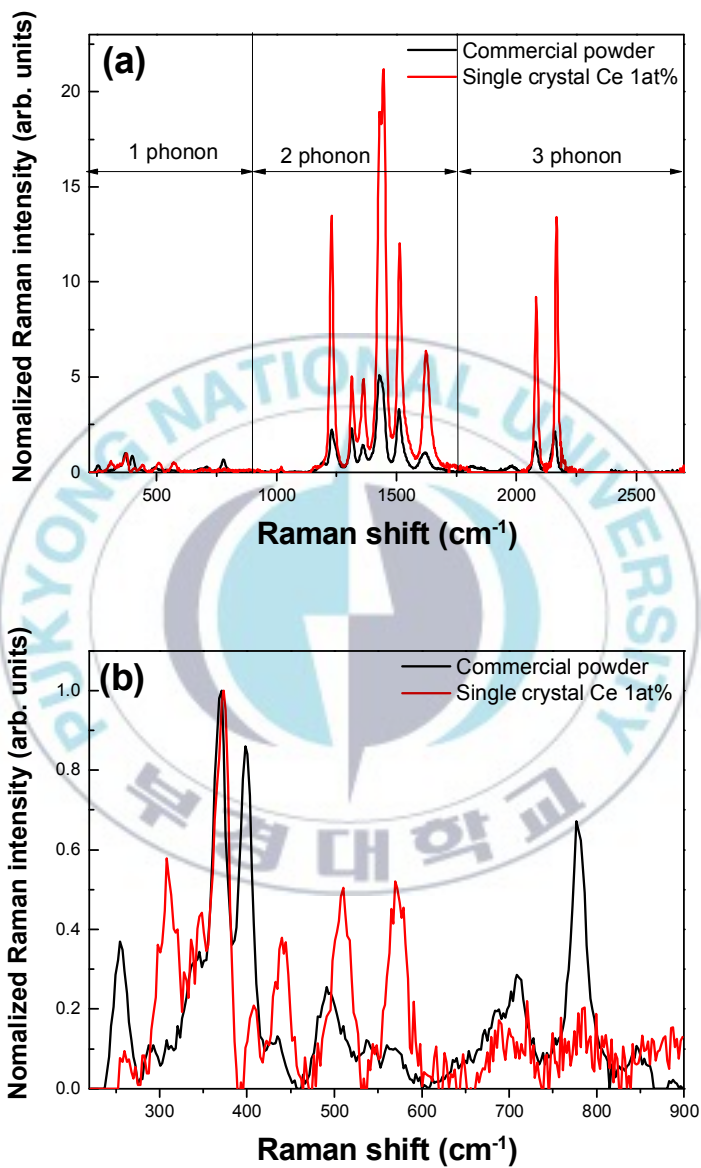


**Fig. 12.** Temperature dependent PL spectra of (a) single-crystal, (b) poly-crystal, and (c) temperature dependence of the relative PL intensity

Generally, the optical/electronic interactions between  $\text{Ce}^{3+}$  ion and the host lattice are dominated by the multi-phonon process. Therefore, the changes of lattice vibration will directly influence the spectral shape and luminescence performance of YAG:Ce crystal.

Figure 13 shows Raman spectra of single-crystal and poly-crystal YAG:Ce phosphors. Raman spectrum of YAG host contains 25 phonon modes ( $3A_{1g}+8E_g+14T_{2g}$ ), and its infrared spectrum contains 17  $T_{1u}$  modes [17]. Almost Raman peaks observed in our experiment are assigned. The Raman peak position and width of the single crystal are almost same as those of the powder. The relative Raman intensities of the single crystal are significantly different from the powder. The Raman peaks at 308, 439, 510, 569  $\text{cm}^{-1}$  have higher intensity, but those at 260, 398, 776  $\text{cm}^{-1}$  show lower intensity, when normalized at the highest peak in 1phonon range and compared with the powder. The experimental Raman shifts along with the calculated ones for the  $\text{Y}_3\text{Al}_5\text{O}_{12}$  are presented in Table 3 [18].





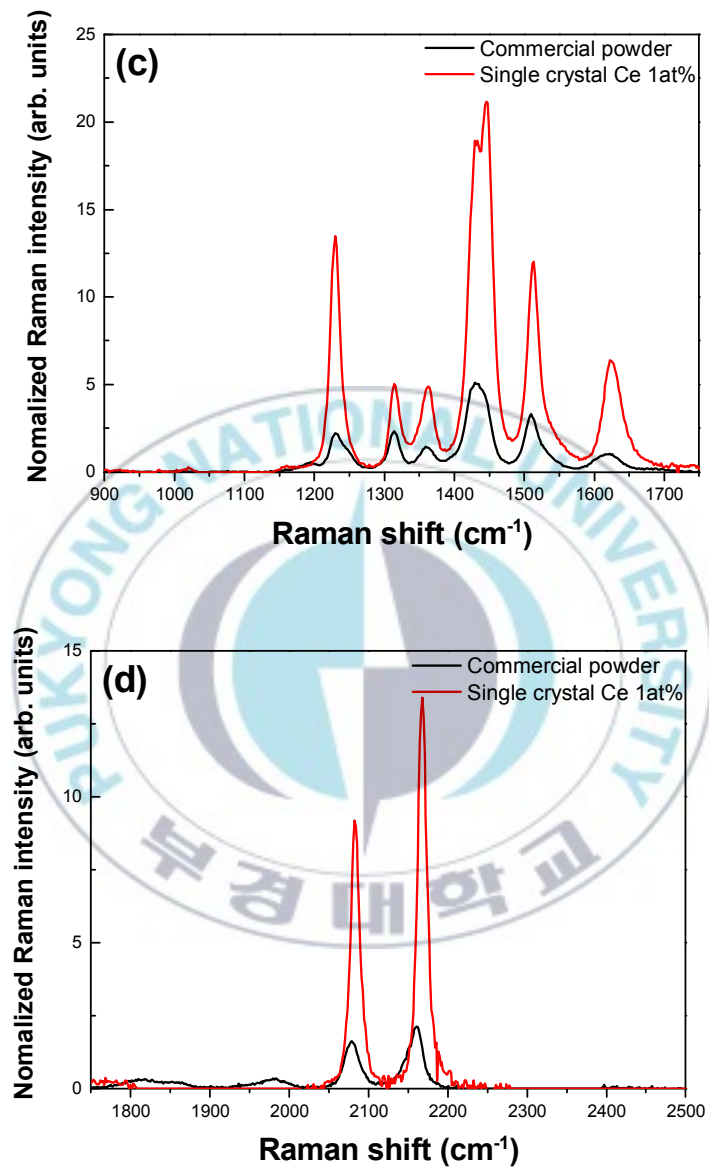


**Fig. 13.** Comparison with Raman spectra of single-crystal and poly-crystal YAG:Ce phosphors at (a) total, (b) 1 phonon, (c) 2 phonon, and (d) 3 phonon range

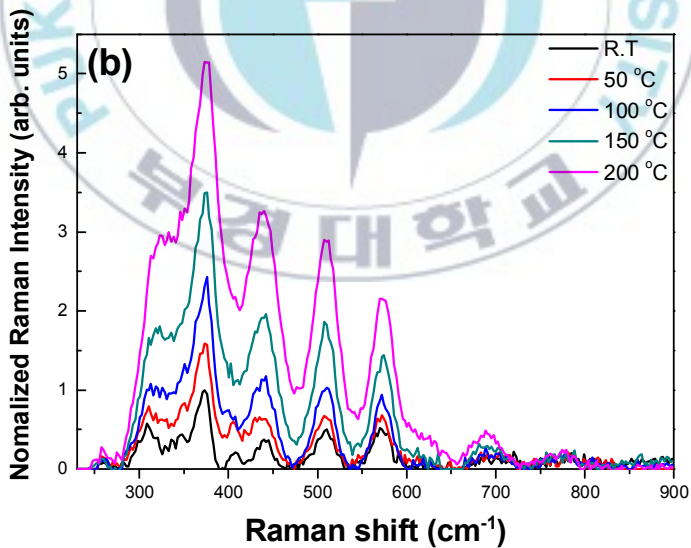
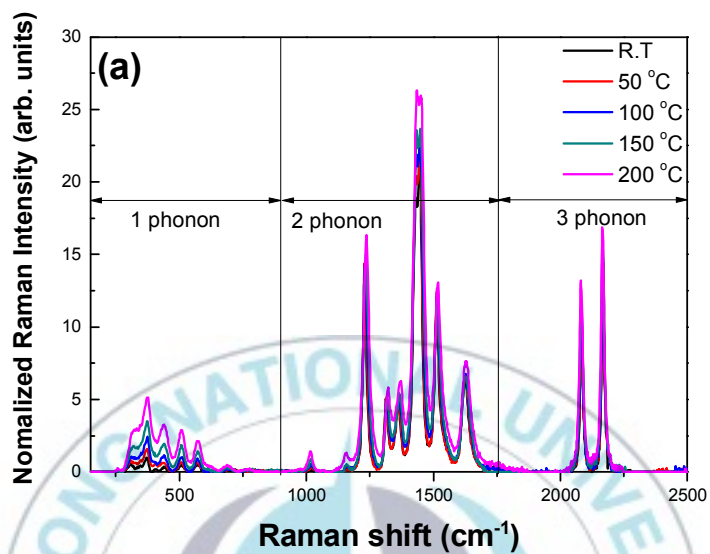
**Table. 3.** Comparison between experimental and calculated [18] Raman-active shifts in 1 phonon range

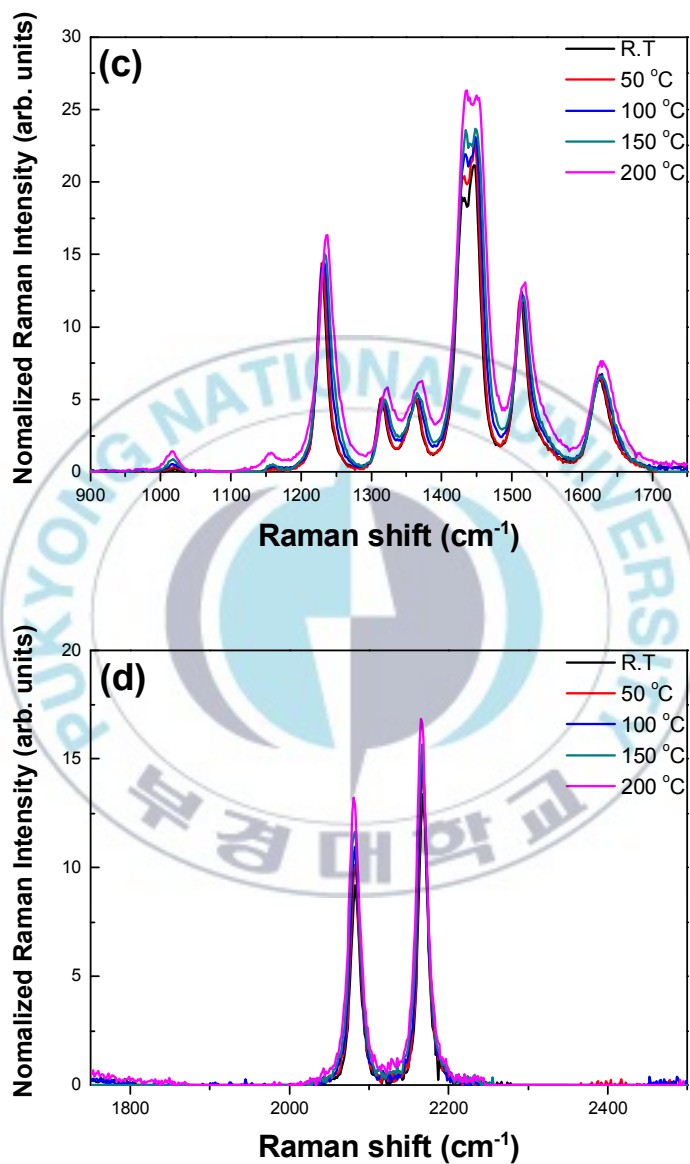
Mode symmetry	$\omega_i$ (exp)	$\omega_i$ (calc)
	(cm <sup>-1</sup> )	
<b>A<sub>1g</sub></b>	373	387
	569	569
	776	776
<b>E<sub>g</sub></b>	-	161
	308	261
	335	360
	422	386
	510	545
	543	633
	688	736
	758	803
	-	137
<b>T<sub>2g</sub></b>	-	214
	-	239
	260	254
	328	289
	348	353
	407	386
	439	477
	466	499
	590	594
	616	661
	709	705
	720	738
	845	886

Temperature-dependent Raman spectra of single-crystal and poly-crystal are shown in Figure 14, 15. As an increase of temperature, Raman intensity of all one-phonon modes of the single crystal are gradually increased together with slight broadening, but their peak positions are not changed.

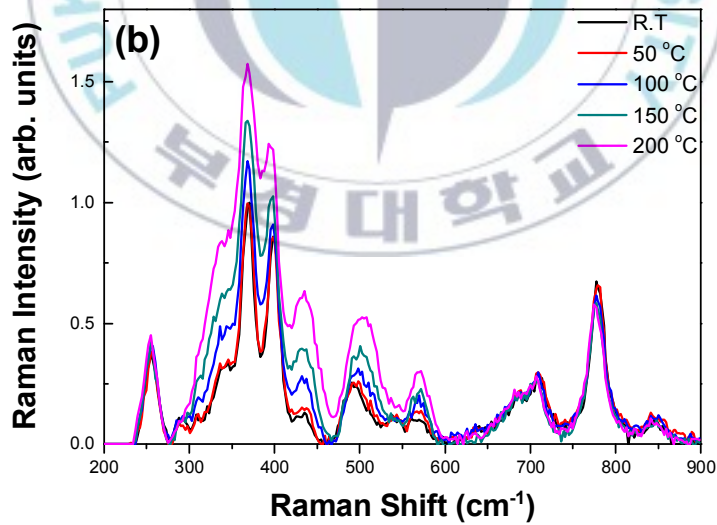
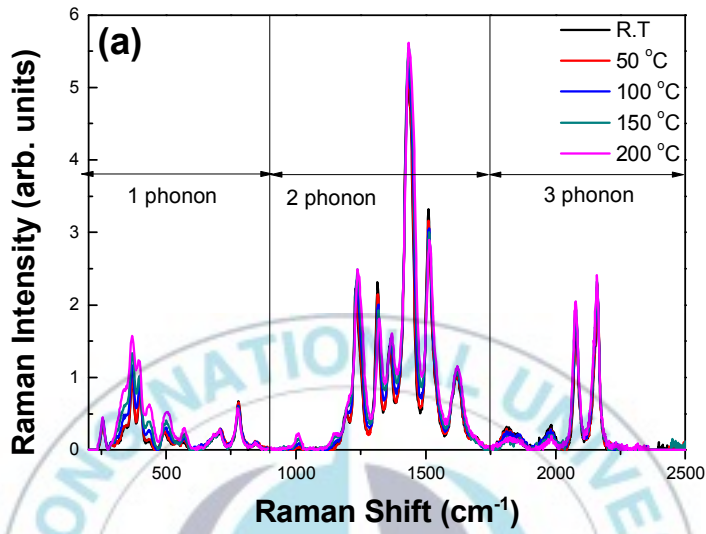
It is able that Raman multi-phonon modes of the single crystal show a drastic intensity enhancement by a factor of 2, compared with the powder sample. The six lines of two-phonon modes are located at 1229 (= 776 + 439), 1313 (= 776 + 543), 1363 (= 688 + 709), 1445 (= 709 + 720), 1513 (= 776 + 720), and 1622 (= 776 + 845)  $\text{cm}^{-1}$  [19]. As an increase of temperature, the Raman intensity of six two-phonon modes are slightly increased with broadening, but their peak positions are gradually shifted to the higher energy side by approximately  $10 \text{ cm}^{-1}$ .

The two lines of three-phonon modes at 2082 (= 688 + 709 + 688) and 2167 (= 688 + 709 + 776)  $\text{cm}^{-1}$  [19] are shifted to the higher energy side by  $5 \text{ cm}^{-1}$ , and their half widths are increased to  $10 \text{ cm}^{-1}$ , compared with the powder. Additional two lines of three-phonon modes in the powder are observed at 1700 - 2000  $\text{cm}^{-1}$  range, but they disappear in the single crystal. As an increase of temperature, the Raman intensity of two three-phonon modes is slightly increased with broadening, but their peak positions are gradually shifted to the lower energy side by approximately 2-3  $\text{cm}^{-1}$ .





**Fig. 14.** Temperature-dependent Raman spectra of single-crystal YAG:Ce at (a) total, (b) 1 phonon, (c) 2 phonon, and (d) 3 phonon range



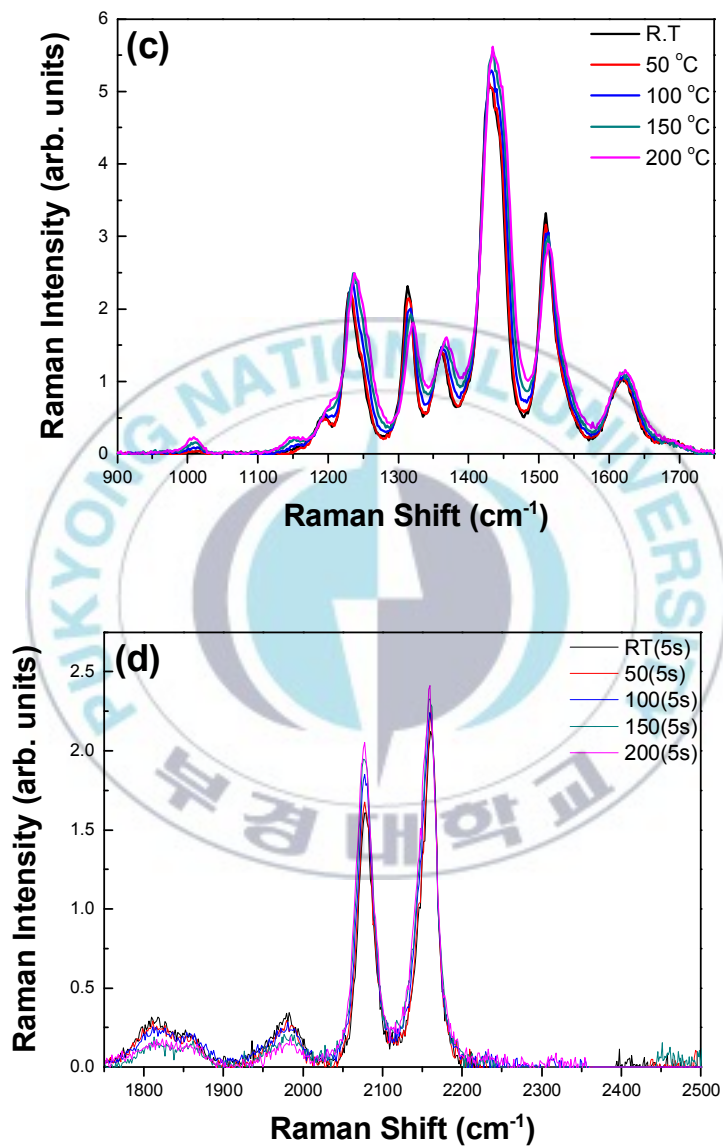


Fig. 15. Temperature-dependent Raman spectra of commercial powder at (a) total, (b) 1 phonon, (c) 2 phonon, and (d) 3 phonon range

The thermal conductivity for the single crystal with no free electron is regarded as the result of the heat transfer by the normal process based on one-phonon modes at lower temperature and Umklapp process based on phonon-phonon interaction at higher temperature than the Debye temperature (TD = 560 K for YAG host). Therefore, the changes of lattice vibration directly influence the thermal conductivity of YAG. The correlation between the thermal conductivity ( $\kappa$ ) and Raman scattering intensity ( $I(\tilde{\nu}_j)$ ) is given as follows [20]

$$\kappa = \frac{B_0 u}{nT^2 F^2} \sum_{j=4}^{3s} \frac{\tilde{\nu}_j^4}{\left(1 - \frac{4\tilde{\nu}_0}{\tilde{\nu}_j}\right)^2 e^{\frac{hc\tilde{\nu}_j}{kT}}} I^2(\tilde{\nu}_j) \quad (1)$$

where  $B_0$  is a constant,  $c$  is the velocity of incident light,  $\tilde{\nu}_0$  is the wavenumber of incident laser  $\nu_0$ , and  $\tilde{\nu}_j$  is the wavenumber of lattice vibration mode  $\nu_j$ ,  $n$  and  $F$  are the concentration and diameter of extended defects as spherical objects.

The comparison with the thermal conductivities of YAG:Ce single crystal, crushed single crystal and commercial power is shown in Table 4. At the room temperature, thermal conductivity of single crystal and crushed single crystal is about 7 times and 2 times larger than commercial sample. As an increase of temperature, thermal conductivities are increased depending on equation (1). The two-phonon modes have the largest effect of total thermal conductivity by the Raman scattering intensity.

**Table 4.** The calculated thermal conductivity ratio

Temperature (°C)	$K_{\text{single}}/K_{\text{commer}}$	$K_{\text{crush}}/K_{\text{commer}}$
25	7.84	2.14
50	9.02	2.32
100	9.98	2.71
150	10.71	3.52
200	14.06	3.75

Figure 16 shows thermographic images of YAG:Ce single-crystal and poly-crystal phosphor-in-glass under 7 Watt blue laser diode. Temperature of single-crystal is 41°C, while poly-crystal is 109°C. Single crystal has lower temperature than poly-crystal. It implies that the thermal conductivity of single crystal is higher than poly crystal.

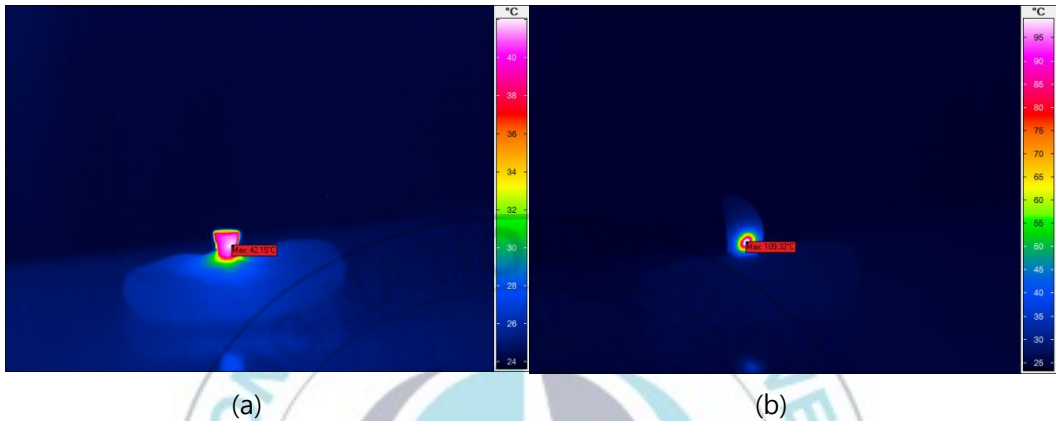


**Fig. 16.** Thermographic images of (a) single-crystal and (b) poly-crystal YAG:Ce

Table 5 demonstrates comparison of the quantum efficiencies (QE) of the single crystal YAG:Ce phosphor, crushed YAG:Ce single crystal powder, commercial powder and YAG glass-ceramic phosphor [21].

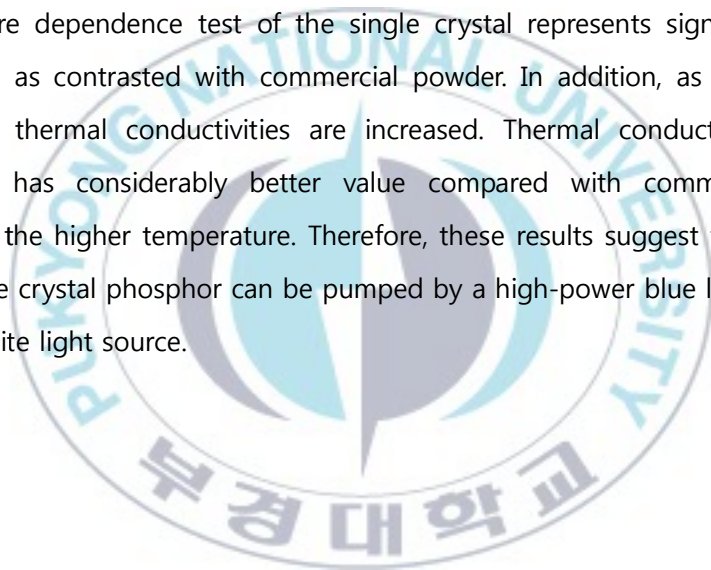
**Table. 5.** Comparison of quantum efficiencies of the single crystal YAG:Ce phosphor, crushed single crystal powder, commercial powder and YAG-GC phosphor

	Commercial powder	Single crystal	Crushed single crystal	YAG glass-ceramic phosphor [21]
Q.E	0.8	0.49	0.7	0.28 - 0.4

## 5. Conclusions

Yellow-emission YAG:Ce single crystal has been grown by the floating zone (FZ) method. Optical and thermal properties of single crystal YAG:Ce as phosphor in comparison to the commercial YAG:Ce powder showed different values and improved stability under the high temperatures. Single crystal in the emission band excited in the blue region (450 nm) has red-shift with increasing Ce<sup>3+</sup> concentration and blue-shift with replacing the Y sites by the Lu ions.

Temperature dependence test of the single crystal represents significantly better characteristic as contrasted with commercial powder. In addition, as an increase of temperature, thermal conductivities are increased. Thermal conductivity of single crystal also has considerably better value compared with commercial sample, especially at the higher temperature. Therefore, these results suggest that the yellow YAG:Ce single crystal phosphor can be pumped by a high-power blue laser diode and LED for a white light source.



## References

- [1] Schubert, E.F. "Light Emitting Diodes", Cambridge, Cambridge University Press. (2003).
- [2] L. S. Rohwer and A. M. Srivastava, *Electrochem. Soc. Interface*, **12** (2003) 36-39.
- [3] G. Fasol, S. Nakamura, Berlin, Springer. (1997).
- [4] N. Narendran, Y. Gu, J.P. Freyssonier, H. Yu, and L. Deng, *J. Cryst. Growth*, **268** 449-456.
- [5] S. Nishiura, S. Tanabe, K. Fujioka, Y. Fujimoto, *Opt. Mater*, **33** (2011) 688-691.
- [6] S. Fujita, S. Yoshihara, A. Sakamoto, S. Tanabe, Fifth International Conference on Solid State Lighting. Proc. of SPIE, (2005) 59411.
- [7] A. Latynina, M. Watanabe, D. Inomata, K. Aoki, Y. Sugahara, E.G. Villora, K. Shimamura, *J. Alloys. Comp*, **553** (2013) 89-92.
- [8] W. Ding, J. Wang, M. Zhang, Q.Zhang, Q. Su, *Chem. Phys. Lett.* 435 (2005) 301.
- [9] Nakamura, S., Mukai, T., and Senoh, M., *Appl. Phys. Lett.*, 64 (1994) 1687-1689
- [10] Shelyapina, M. G., Kasperovich, V. S., Wolfers, P., *J. Phys. Chem. Solids*, 26 (2006) 720-724.
- [11] Blasse, G., Wanmaker, W.L., Tervrugt, J.W., and Brill, A., *Philips Res. Rept.*, 23 (1968) 189.
- [12] T. Mizutani, K. Matsumi, H. Makino, T. Yamamoto, T. Kato, *NEC Res. Dev.* 33 (1974) 86.
- [13] A. Cröll, *German Assoc. Cryst. Growth (DGKK) Newslett.* 65 (1997) 13-22.
- [14] B. N. Roy, *Adv. Mater.* 4 (1992) 694.
- [15] S.M. Koohpayeh, D. Fort, J.S. Abell, *Prog. Cryst. Growth. Ch.* 54 (2008) 121-137
- [16] T. Duffar, "Crystal Growth Processes Based on Capillarity", A John Wiley & Sons, Ltd. (2010).
- [17] K. Papagelis, G. Kanellis, S. Ves, and G. A. Kourouklis, *Phys. Stat. Sol.* 223 (2002) 134-150

- [18] P. Goel, R. Mittal, N. Choudhury, and S. L. Chaplot, *J. Phys. Condens. Matter.* 22 (2010) 065401
- [19] G. A. Slack, D. W. Oliver, R. M. Chrenko, and S. Roberts, *Phys. Rev.* 177 (1969) 3
- [20] G. Lu, C. Li, W. Wang, Z. Wang, H. Xia, P. Zhao, *Mat. Sci. Eng. B.* 98 (2003) 156-160
- [21] S. Fujita, A. Sakamoto, and S. Tanabe, *IEEE J. Sel. Top. Quantum Electron.* 14 (2008)



## 국문 요약

# 고출력 LD/LED용 황색 YAG:Ce 단결정 형광체

## 강 태 욱

### 부경대학교 대학원 재료공학과

#### 요 약

황색을 발광하는  $Y_3Al_5O_{12}:Ce$  (YAG:Ce) 단결정 형광체를 floating zone 법으로 성장시키고 연구를 진행하였다. YAG 단결정은 결정구조내의 {110}의 결정방향으로 성장시켰다. 이 단결정 형광체는 450 nm의 청색광을 여기했을 때 황색광을 발광하고 540 nm의 최대 발광파장과 75 nm의 반치폭을 가진다. Y의 자리에 Lu이 치환되면 발광파장은 녹색으로 이동되고, 이는 치환되는 Lu의 농도가 많아질수록 더 많이 이동된다. 이러한 YAG:Ce 단결정 형광체의 광학적, 열적 특성은 기존에 상용화된 YAG:Ce 분말과 함께 비교했다. 이러한 열전도율은 격자진동에 관련이 있고, 라만 스펙트럼 측정을 통해 단결정의 라만 강도가 크다는 것을 확인하고 열전도율을 계산하고 비교하였다. 단결정 형광체는 열전도율이 높아서 고출력의 레이저 다이오드에 의한 발광에서 열적 안정성이 우수하다.

---

핵심이 되는 말 :  $Y_3Al_5O_{12}:Ce$  형광체, 단결정, 온도 소광, , floating zone 법, 레이저 다이오드

## 감사의 글

2년동안의 석사과정을 마치며, 그 동안 도움을 주신 많은 분들에게 감사의 마음을 전하고자 이 글을 적습니다.

먼저 지난 5년 연구실에 속해있는 동안 정말 많은 지도와 앞으로의 길을 열어갈 수 있도록 도움을 주신 제 마음 속 스승이신 최희락 교수님께 진심으로 머리 숙여 깊은 감사를 드립니다.

저의 석사과정 동안의 연구를 함께 하며 많은 지도편달과 진심 어린 충고를 아끼지 않으시고 열정을 불어 일으켜 주셨던 저의 멘토이신 김종수 교수님께도 진심으로 감사를 드립니다.

항상 열심히 하라는 격려와 지도를 해주시는 박찬 교수님, 자기관리와 사고의 중요성을 일깨워 주신 정해용 교수님, 연구장비와 연구기반을 마련해주신 유영문 센터장님께 감사드립니다.

운이 좋아 좋은 사람들 만나 5년동안 즐겁게 생활해 온 전자세라믹스 실험실.

항상 유쾌하고 추진력 넘치시는 다일이 행님, 섬세하게 많이 챙겨주던 영은이, 신미진, 5년을 꼭 함께해 온 든든한 동생 재훈이, 늦게 들어왔지만 항상 열심히 하는 헌태, 형 마음 잘 알아주고 성격도 비슷해서 친동생 같은 택이, 마음이 어려서 걱정이고 챙겨주고 싶은 동생 영민이, 영우, 똘끼 있는 귀여운 태성이, 말썽쟁이 현수, 실험실에 활력을 불어넣어주는 귀여운 선화와 김미진, 들어온 지 얼마 안됐지만 열심히 하는 정훈이, 모두들 정말 감사하고 항상 건강하고 앞으로 하는 일 잘 되기만을 바랍니다. 그리고 자주 뵙지는 못하지만 가끔씩 찾아와 많은 도움을 주신 실험실 선배님들에게도 감사의 말씀 드립니다.

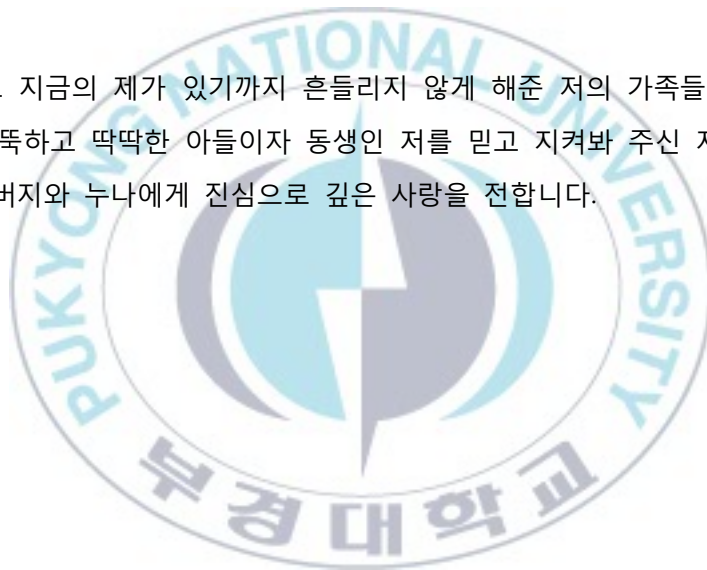
일일이 언급하기에 너무 많은 재료과 실험실 선후배님들 모두에게도 감사를 드립니다. 특히, 복학 후 학교생활에 쉽게 적응할 수 있었던 조교쌤 석환이 행님과 태균이 행님, 그리고 함께 놀고 공부했던 선배님들에게 감사드립니다.

또 저와 함께 2년간의 석사과정을 마무리하는 저의 동기들, 항상 든든하게 중심 잡아주시는 재호행님, 함께 조교도 하며 즐거운 시간 많이 보냈고 좋은 동생 경쿠, 내가 챙겨준다고 고생했던 해인이, 다들 감사하고 앞으로도 열심히 합시다.

늦게 친해지게 되었지만 정말 열심히 연구에 매진하는 이미지시스템공학과 발광연구실. 늦게 알게 되었지만 마음 통하고 많은 가르침 주시며, 저를 좋게 봐주셔서 더 감사한 광원선배, 항상 열심히 하시고 덕분에 많이 배우게 되는 배울 점 많은 형석선배, 적응하는데 도움주시고 재미있게 지냈던 성우선배, 힘든 일도 묵묵히 하며 예의바르고 착한 석규와 대한이, 부족하지만 착하고 재밌는 재형이까지, 함께 한 시간은 아직 길지 않지만 정말로 깊은 감사를 드립니다.

지치고 힘들 때 힘이 되어준 친구들. 불 같은 성격이지만 마음은 착하고, 덕분에 심심하지 않은 사고몽치 재광이, 그저 착하고 여린 외모지상주의 망구, 이제서야 정신차리기 시작한 동기 두치, 이외에도 함께해 준 친구들에게 감사하고 하는 일들 잘되길 바란다.

마지막으로 지금의 제가 있기까지 흔들리지 않게 해준 저의 가족들에게 감사를 전합니다. 무뚝뚝하고 딱딱한 아들이자 동생인 저를 믿고 지켜봐 주신 저의 안식처이자 버팀목인 아버지와 누나에게 진심으로 깊은 사랑을 전합니다.



**2015년 1월**  
**강태욱 드림.**